Supporting Information

Synthesis of two tetra-azolium salts and the recognition performance for guests

Zhi-Xiang Zhao,[a] Lin-Hai Hu,[a] Shao-Cong Yu[a] and Qing-Xiang Liu*[a]

[a] *Tianjin Key Laboratory of Structure and Performance for Functional Molecules, College of Chemistry, Tianjin Normal University, Tianjin 300387, P. R. China.*

* *Corresponding author, E-mail: tjnulqx@163.com*

List of the contents

1. CCDC number for compound 1.

CCDC 2161181 for **1** contains the supplementary crystallographic data. The data can be obtained free of charge via http//www.ccdc.cam.ac.uk/conts/retrieving.html, or from the Cambridge Crystallographic Data Centre, 12 Union Road, Cambridge, CB2 1EZ, UK; fax: (+44) 223-336-033; or e-mail: deposit@ccdc.cam. ac. uk.

2. Summary of crystallographic data for 1.

Table S1 Summary of crystallographic data for **1**

Chemical formula	$C_{62}H_{54}F_{24}N_{12}P_4$	$F(000)$	786.0
Fw	1547.05	Cryst size, mm	0.25 × 0.24 × 0.23
Cryst syst	triclinic	θ_{min},θ_{max},deg	3.74, 50.012
Space group	P-1	T /K	149.7(9)
a/Å	11.7095(6)	No. of data collected	11506
b/Å	12.1400(6)	No. of unique data	5748
c/Å	12.8528(8)	No. of refined params	460
α/°	74.284(5)	Goodness-of-fit on F^{2a}	1.028
β/°	69.199(5)	Final R indices[b] [I> $2\sigma(I)$]	
γ/°	79.296(4)	$R1$	0.0587
V/Å^3	1635.97(17)	$wR2$	0.1489
Z	1	R indices (all data)	
D_{calcd},Mg/m^3	1.570	$R1$	0.0791
Abs coeff, mm^{-1}	0.236	$wR2$	0.1654

[a]$GOF = [\Sigma\omega(F_o^2 - F_c^2)^2/(n-p)]^{1/2}$, where n is the number of reflection and p is the number of parameters refined. [b]$R_1 = \Sigma(||F_o| - |F_c||)/\Sigma|F_o|$; $wR_2 = [\Sigma[w(F_o^2 - F_c^2)^2]/\Sigma w(F_o^2)^2]^{1/2}$.

3. The crystal packing of 1.

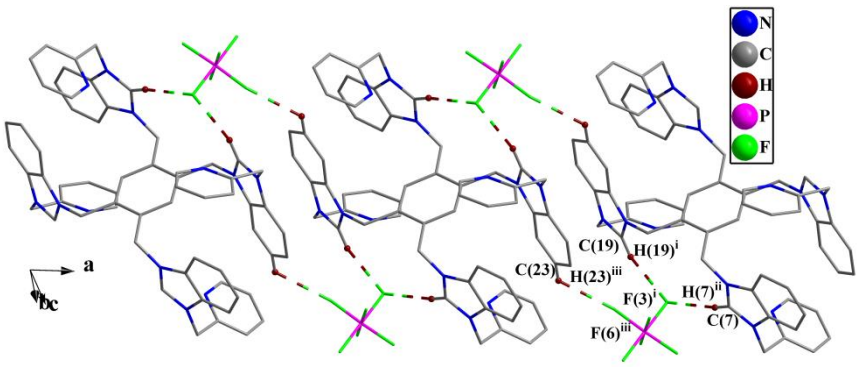

Fig. S1 1D polymeric chain of compound **1**.

4. H-Bonding Geometry (Å, ˚) for 1.

Table S2. H-Bonding Geometry (Å, ˚) for **1**

	D-H···A	D-H	H···A	D···A	D-H···A
1	C(1)9-H(19)···F(3)^{i}	0.930(1)	2.547(4)	3.339(1)	143.2(7)
	C(7)-H(7)···F(3)^{ii}	0.930(1)	2.430(2)	3.328(2)	162.3(8)
	C(23)-H(23)···F(6)^{iii}	0.930(1)	2.588(6)	3.179(5)	121.8(6)

Symmetry code: i: 2-*x*, 1 -*y*, - *z*; ii: 2-*x*, 1 -*y*, 1-*z*; iii: 2-x, 1-y, 1-z for **1**

5. Fluorescence experiments, UV/Vis experiments and Job's plot

5.1 Fluorescent experiments

The stock solutions of hosts and guests (5.0×10^{-4} mol/L for host and 5.0×10^{-3} mol/L for guest) were prepared via dissolving the host or the guest in CH_3CN at 25 ˚C. Test solutions were prepared via putting the host stock solution (0.1 mL) or the appropriate amount of the guest stock solution in a 10 mL volumetric flask, which were diluted to 10 mL. In the test solutions, the concentrations of the guest were from 0 to 30×10^{-6} mol/L for **1** and 0 to 15×10^{-6} mol/L for **2**. The samples were excited at 260 nm for **1** and 318 nm for **2**.

The stock solution of NO was prepared by dissolving diethylamineNONOate (DEA·NONOate) (5.0×10^{-3} mol/L, a NO-releasing reagent) in NaOH solution (0.01 mol/L), and test solutions were prepared via putting the host stock solution (0.1 mL) or the appropriate amount of the guest stock solution in a 10 mL volumetric flask with phosphate-buffered saline (PBS) solution (pH 7.4). In the test solutions, the concentrations of DEA·NONOate were from 0 to 30×10^{-6} mol/L. After an incubation of 10 min, the fluorescent intensity was recorded.

5.2 UV experiments

In UV experiments, the stock solutions and test solutions were prepared in the ways that are similar to the fluorescent experiments. The concentration of host was 1.0×10^{-5} mol/L, and the concentrations of the guest were from 0 to 22.5×10^{-6} mol/L for **1** and 0 to 6×10^{-6} mol/L for **2**.

5.3 Method of Job's plot

In Job's plot experiments, the stock solutions and test solutions were prepared in the ways that are similar to the fluorescent experiments. In the experiments, the fixed total concentration (1.0×10^{-5} mol/L) was kept, and the molar fractions of guests were in the range of 0-1.

6. The UV/Vis spectra, fluorescence spectra, HRMS, IR spectra of 1, OPD and 1·OPD

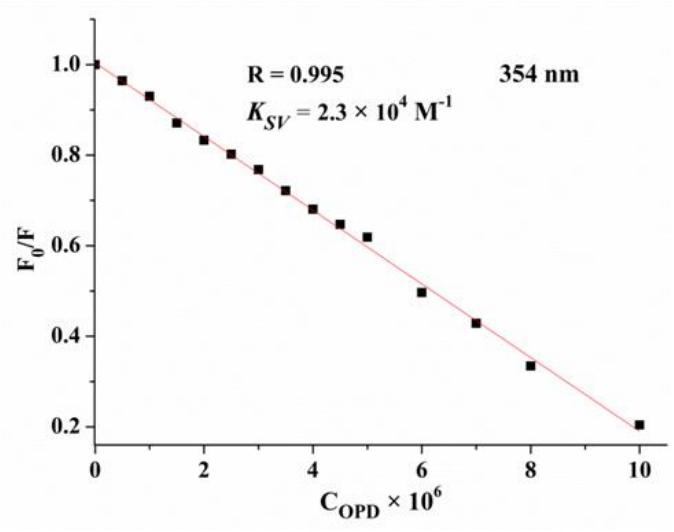

Fig. S2 Stern-Volmer plot describing **1** increasing caused by OPD association in CH_3CN at 354 nm. The K_{SV} is 2.3 × 10^4 M^{-1}, and the linear range is from 0-10.0 × 10^{-6} mol/L.

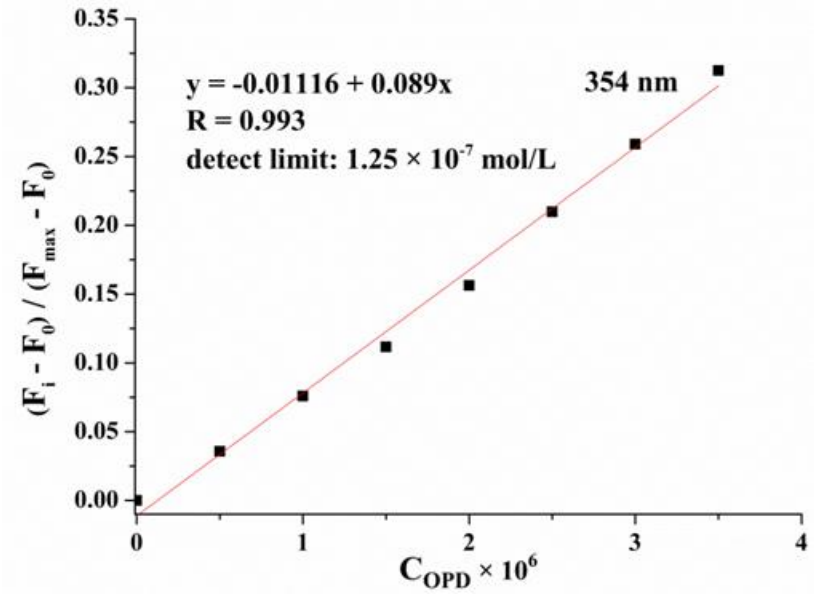

Fig. S3 Emission of **1** at different concentrations of OPD (0, 0.5, 1, 1.5, 2.0, 2.5, 3.0, 3.5 × 10^{-6} mol/L) added at 354 nm. The detection limit was determined to be 1.25 × 10^{-7} M.

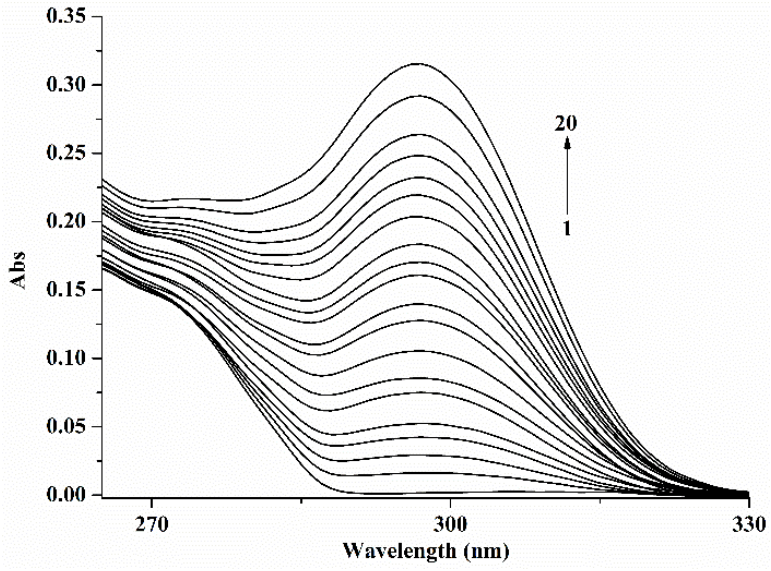

Fig. S4 UV/vis titration spectra of **1** (1×10^{-5} mol/L). C_{OPD} are 0, 0.5, 1, 1.5, 2.0, 2.5, 3.0, 3.5, 4.0, 4.5, 5.0, 6.0, 7.0, 8.0, 10, 12.5, 15, 17.5, 20, 22.5×10^{-5} mol/L.

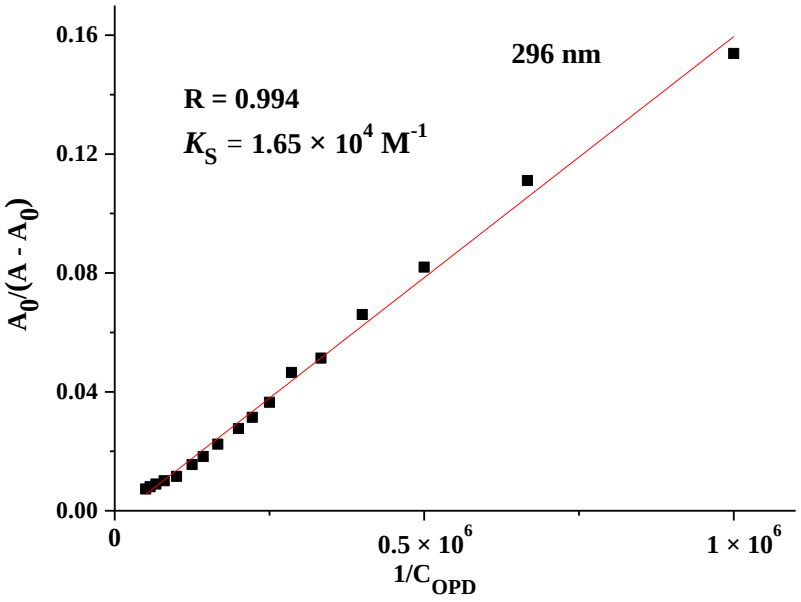

Fig. S5 Linear relationship between $A_0/(A_0 - A)$ versus $1/C_{OPD}$ based on the standard equation: Benesi-Hildebrand plots at 296 nm.

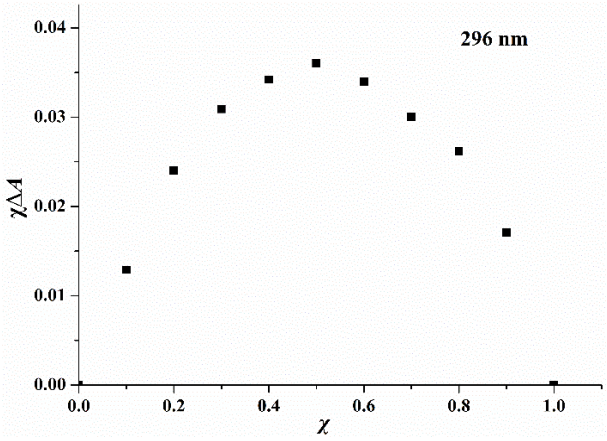

Fig. S6 Job's plot of **1** to OPD in CH_3CN at 296 nm.

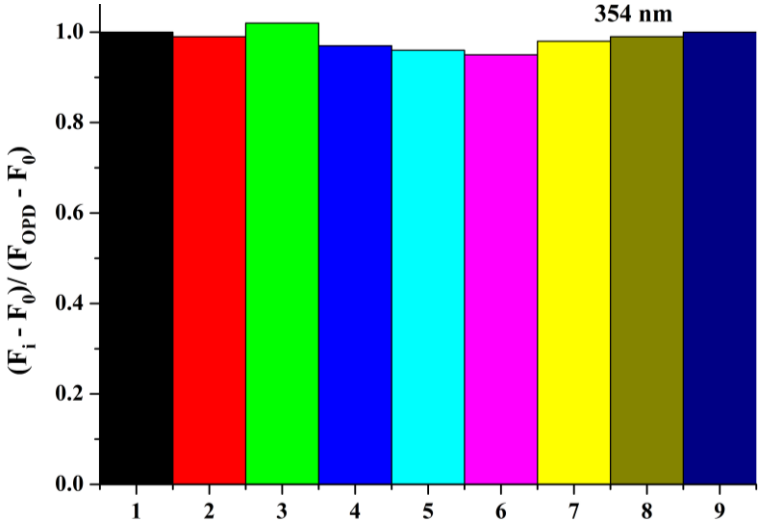

Fig. S7 Change ratio $(F_0 - F_i)/(F_0 - F_{OPD})$ of fluorescence intensity at 354 nm of **1** upon addition of 5 equiv. of OPD in the presence of 5 equiv. of background molecules. (1) OPD; (2) OPD + *m*-phenylenediamine; (3) OPD + *p*-phenylenediamine; (4) OPD + *m*-dinitrobenzene; (5) OPD + *p*-nitrotoluene; (6) OPD + nitrobenzene; (7) OPD + *o*-nitroaniline; (8) OPD + *m*-nitroaniline; (9) OPD + *p*-nitroanilinein CH_3CN at 25 ˚C.

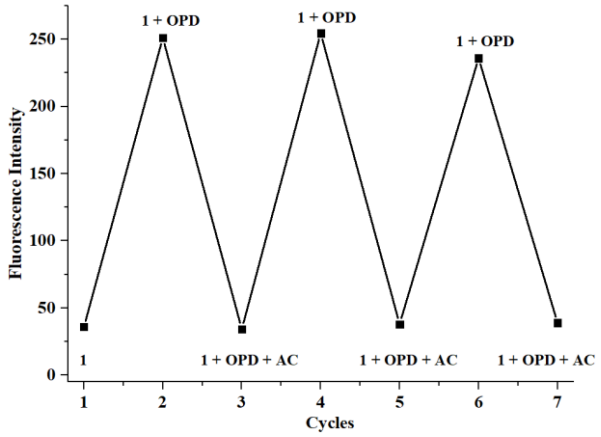

Fig. S8 Reversible behavior of **1** upon the addition of OPD and acetyl chloride (AC).

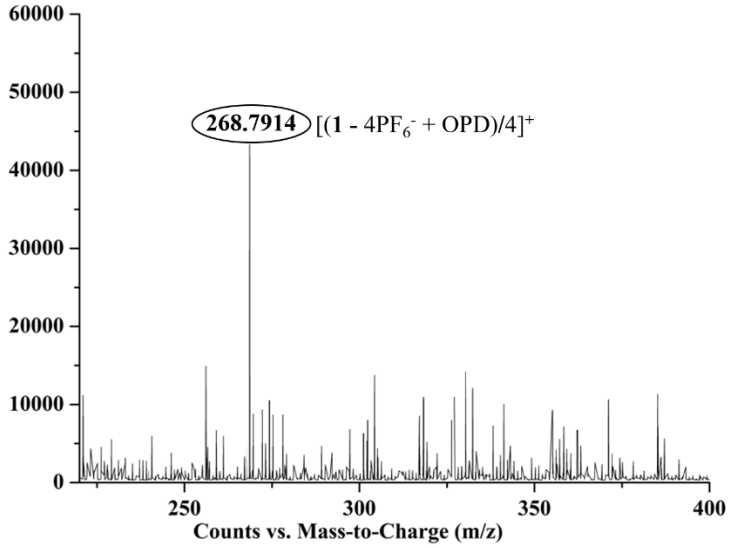

Fig. S9 HRMS spectra for **1**·OPD. MS (EI): $[(\mathbf{1} + \text{OPD} - 4PF_6^-)/4]^+ = 268.7914$.

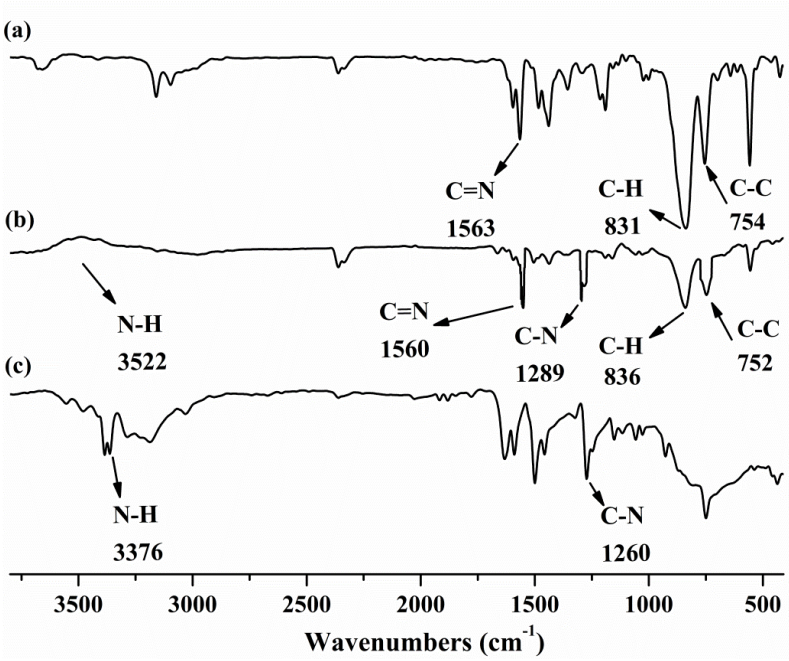

Fig. S10 Infrared spectra of (a) OPD, (b) **1** and (c) **1**·OPD.

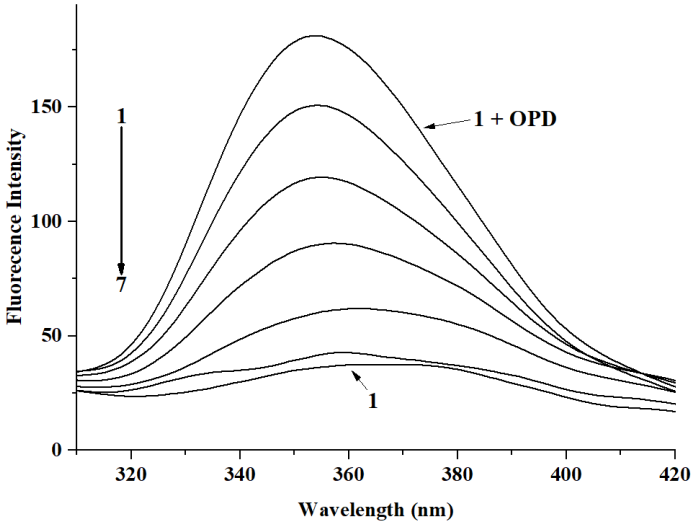

Fig. S11 Fluorescence spectra of **1**·OPD (5×10^{-6} mol/L) upon the addition of DEA·NONOate (0, 5, 10, 15, 20, 25, 30 $\times 10^{-6}$ mol/L) in PBS (phosphate-buffered saline solution (pH 7.4)) buffer solution (λ_{ex} = 260 nm, slit: ex = 5 nm, em = 5 nm).

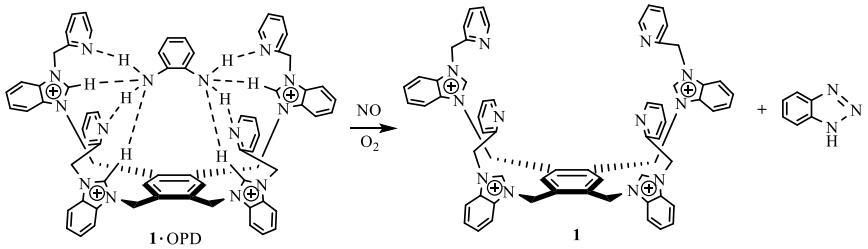

Scheme S1 The reaction between OPD of **1**·OPD and NO.

7. The UV/Vis spectra, fluorescence spectra, HRMS, IR spectra of 2, F^- and 2·F^-

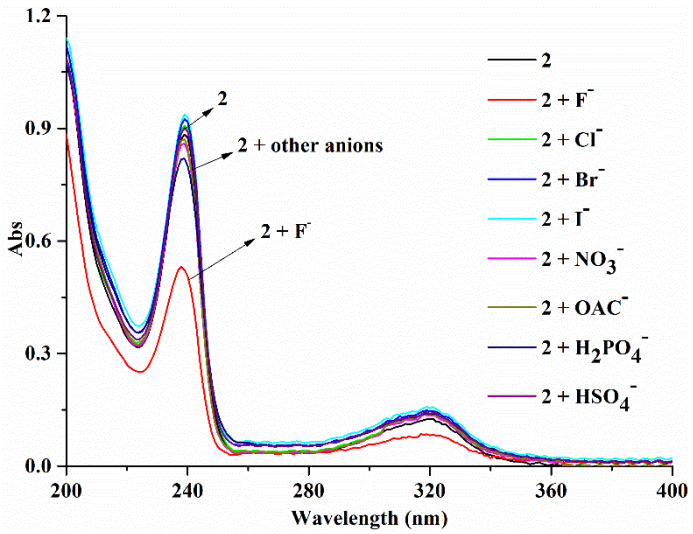

Fig. S12 UV-vis absorption spectra of **2** (1×10^{-5} mol/L) and upon the addition of 2 equiv. of anions F^-, Cl^-, Br^-, I^-, $H_2PO_4^-$, HSO_4^-, OAc^- and NO_3^-, and their cations being tetrabutylammonium (TBA^+) in CH_3CN at 25 ˚C.

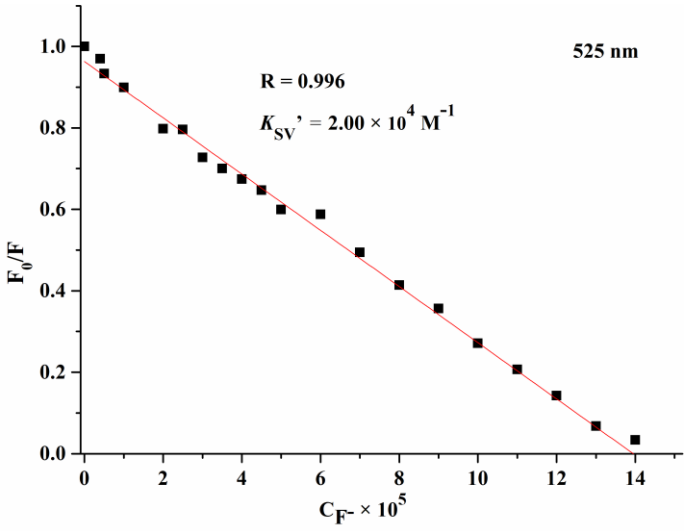

Fig. S13 Stern-Volmer plot describing **2** increasing caused by F^- association in CH_3CN at 525 nm. The K_{SV}' is 2.00 × 10^4 M^{-1}, and the linear range is from 0-13.0 × 10^{-5} mol/L.

$$F_0/F = 1 + K_{SV}'C_{F^-} \qquad (1)$$

where F_0 and F were the fluorescence intensities of **2** in absence and presence of F^-, respectively. C_{F^-} represented the concentration of F^- and K_{SV}' was the association constant.

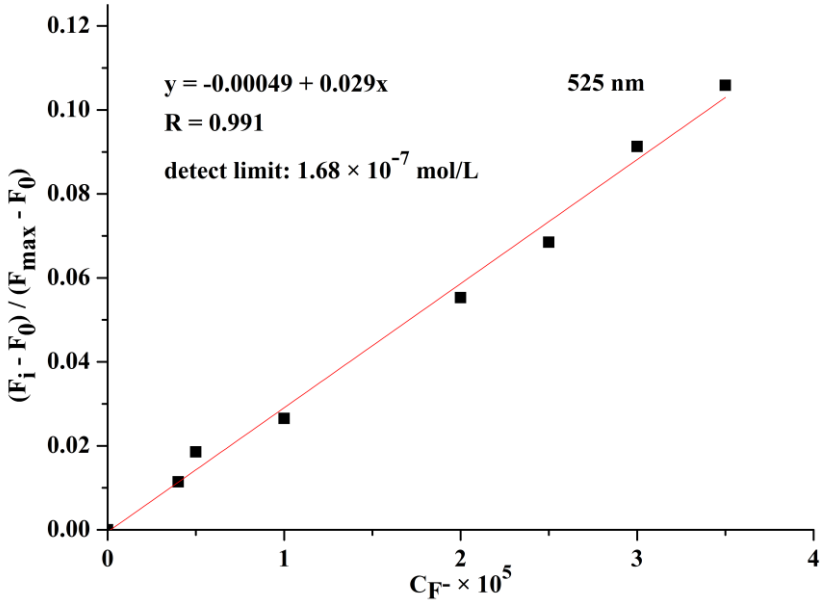

Fig. S14 Emission of **2** at different concentrations of F^- (0, 0.4, 0.5, 1, 2, 2.5, 3, 3.5 × 10^{-5} mol/L) at 525 nm, normalized between the minimum emission (0.0 mol/L of TBAF) and the emission at 3.5 × 10^{-5} mol/L of TBAF. The detection limit was determined to be 1.68 × 10^{-7} M.

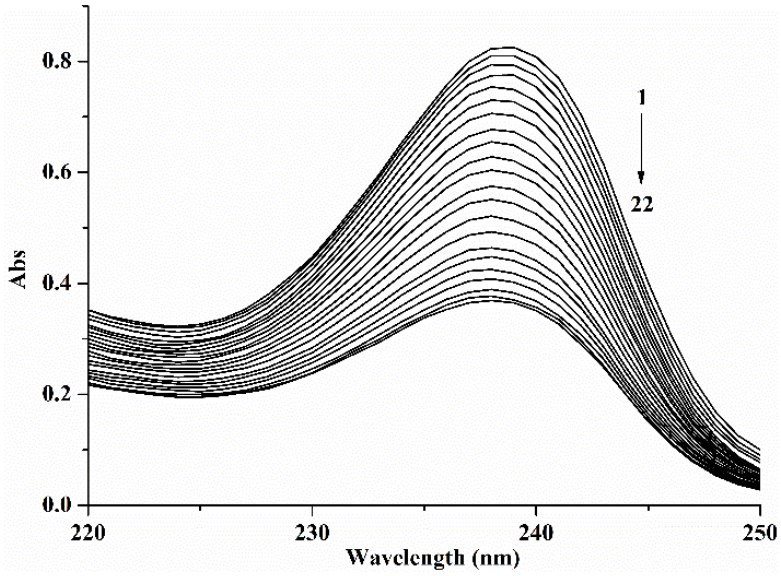

Fig. S15 UV/vis titration spectra of **2** (1.0×10^{-5} mol·L^{-1}). C_{F^-} are 0, 0.1, 0.2, 0.3, 0.45, 0.55, 0.65, 0.75, 0.85, 1, 1.2, 1.4, 1.6, 1.8, 2, 2.5, 3, 3.5, 4, 4.5, 5, 6×10^{-5} mol/L).

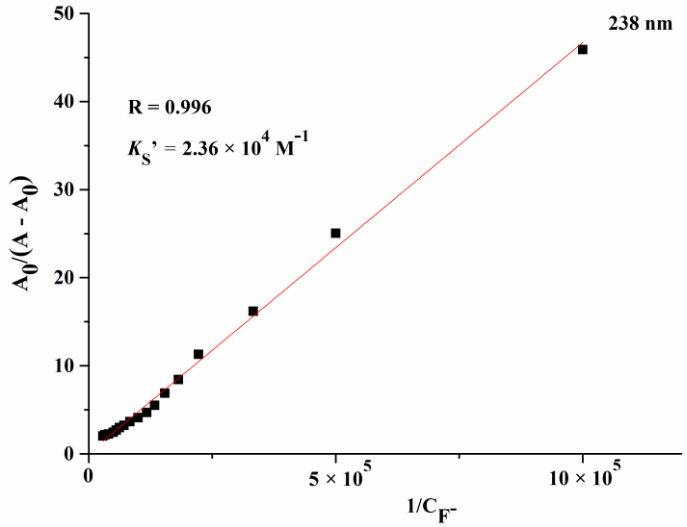

Fig. S16 Linear relationship between $A_0/(A - A_0)$ versus $1/C_{F^-}$ at 238 nm based on the standard equation: Benesi-Hildebrand plots.

$$A_0/(A - A_0) = [\varepsilon_r/(\varepsilon_r - \varepsilon_c)](1/K'C_{F^-} + 1) \qquad (2)$$

where A_0 was the absorbance of **2** without F^- and $A - A_0$ was the discrepancy of absorbances with or without F^-; ε_r and ε_c were the molar extinction coefficients of F^- and **2**·F^-, respectively; C_{F^-} was the concentration of F^-.

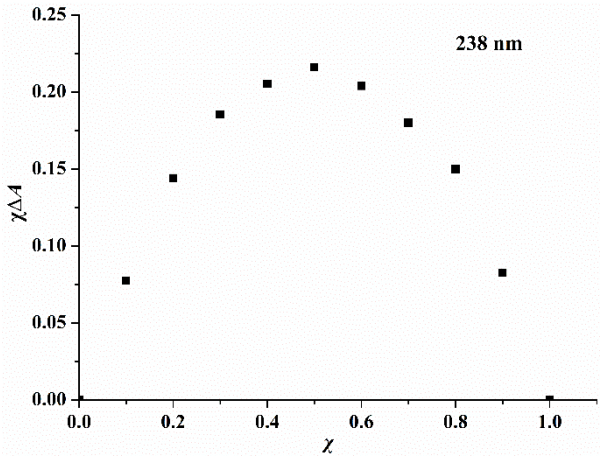

Fig. S17 Job's plot for **2**·F^- in CH_3CN at 238 nm.

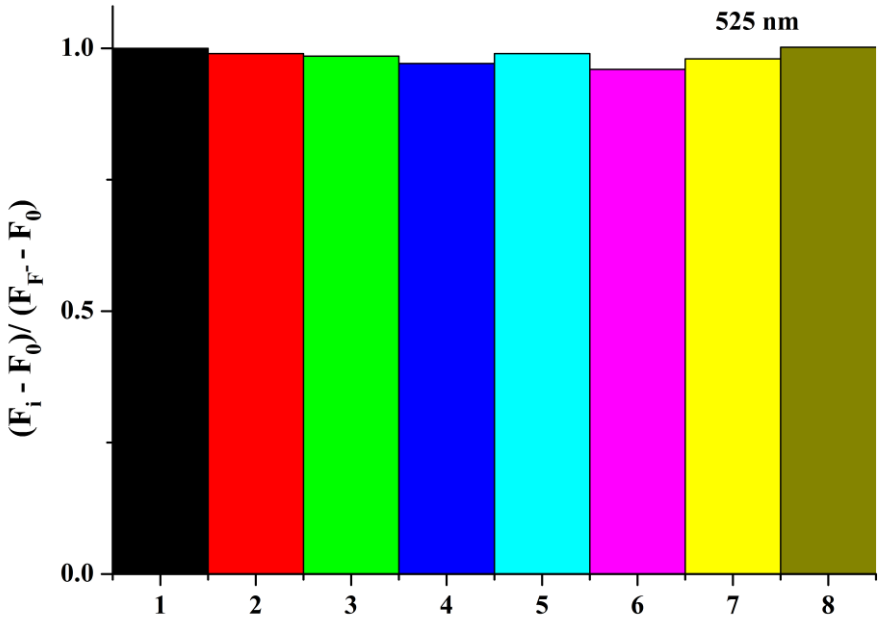

Fig. S18 Change ratio $(F_i - F_0)/(F_{F^-} - F_0)$ of fluorescence intensity at 525 nm of **2** upon addition of 2 equiv. of F^- in the presence of 2 equiv. of background anions. (1) F^-; (2) $F^- + Cl^-$; (3) $F^- + Br^-$; (4) $F^- + I^-$; (5) $F^- + H_2PO_4^-$; (6) $F^- + HSO_4^-$; (7) $F^- + OAc^-$; (8) $F^- + NO_3^-$ in CH_3CN at 25 ˚C.

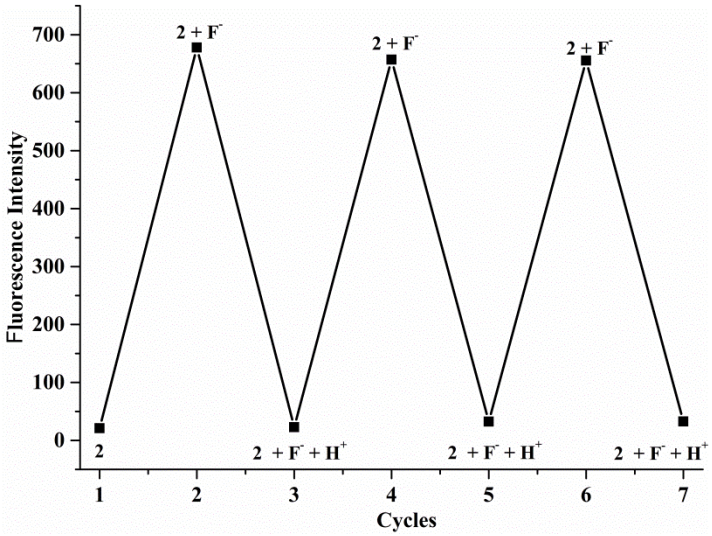

Fig. S19 Reversible behavior of **2** upon the addition of TBAF and TFA.

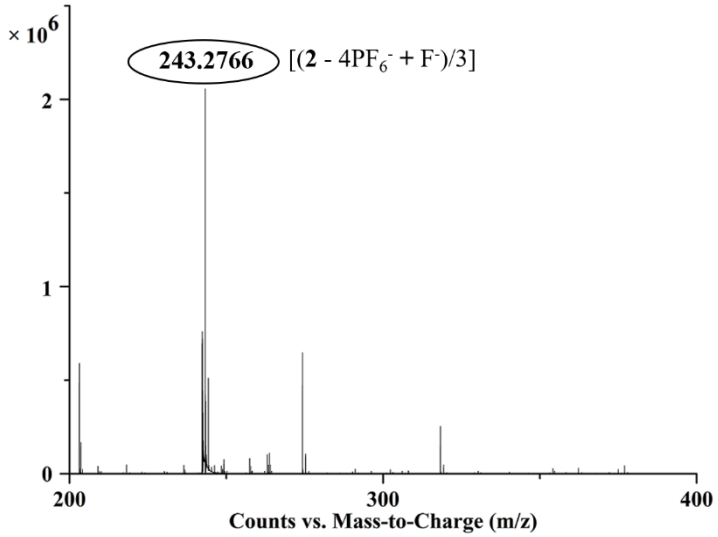

Fig. S20 HRMS spectra for **2**·F^-. MS (EI): $[(\mathbf{2}+ F^- - 4PF_6^-)/3]^+$ = 243.2766.

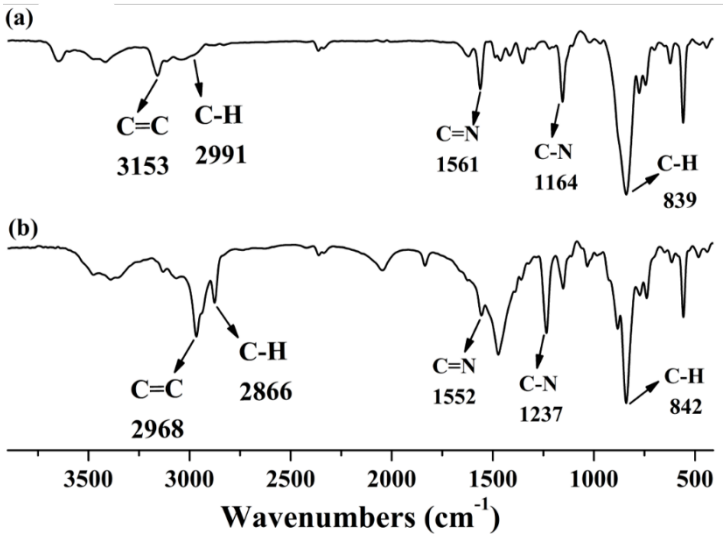

Fig. S21 Infrared spectra of (a) **2** and (b) **2**·F^-.

8. The ^{1}H NMR and ^{13}C NMR spectra of all intermediate, 1 and 2

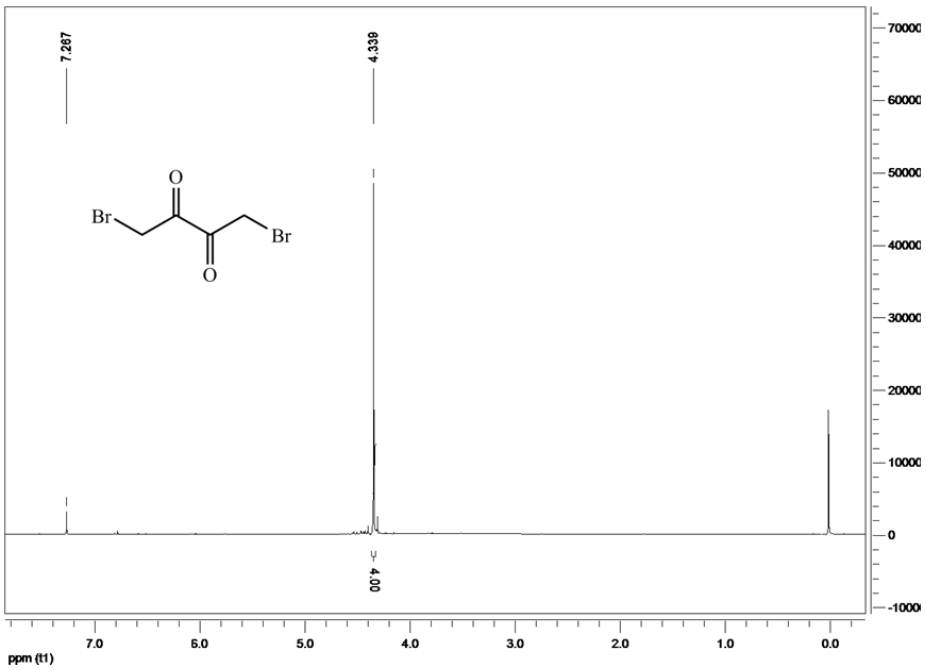

Fig. S22 The ^{1}H NMR (400 MHz, $CDCl_3$) spectrum of 1,4-dibromo-2,3-butanedione.

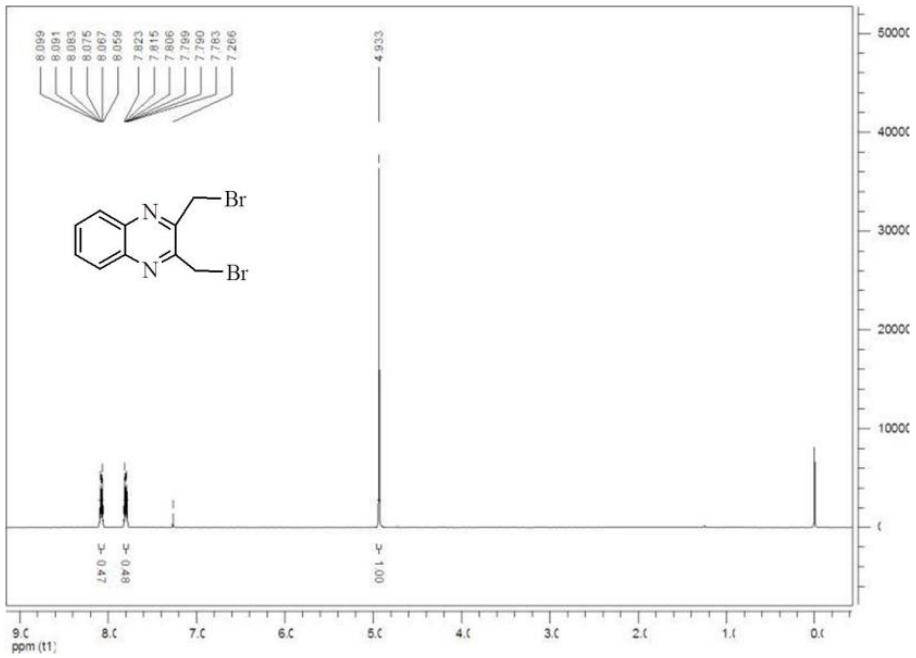

Fig. S23 The ^{1}H NMR (400 MHz, $CDCl_3$) spectrum of 2,3-bis(bromomethyl)quinoxaline.

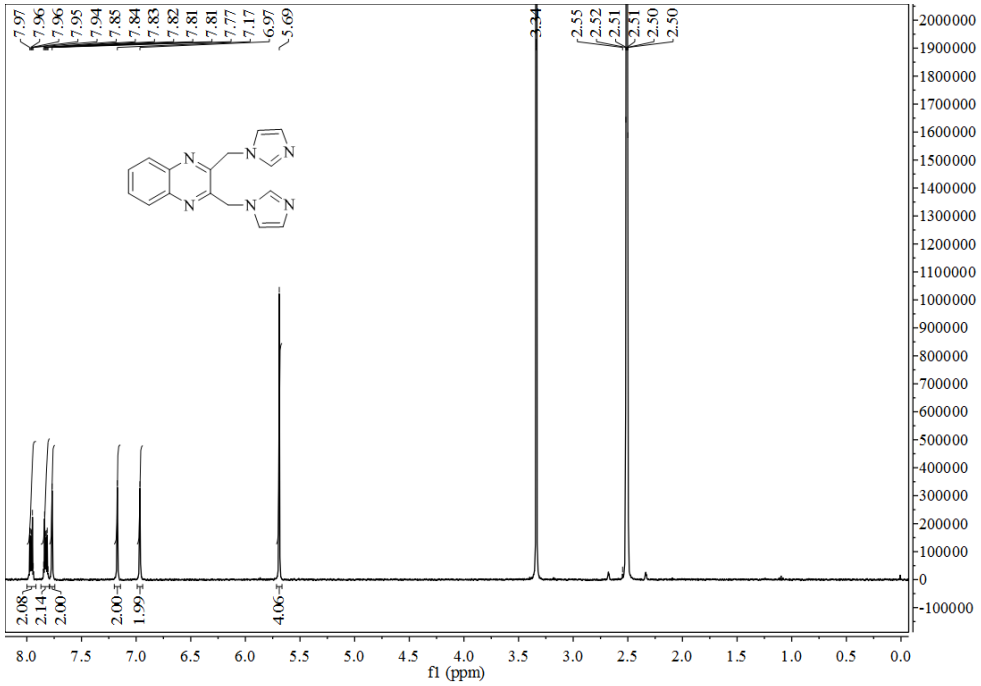

Fig. S24 The ^{1}H NMR (400 MHz, DMSO-d_6) spectrum of 2,3-bis[1'-(imidazol-1''-yl)methyl]quinoxaline.

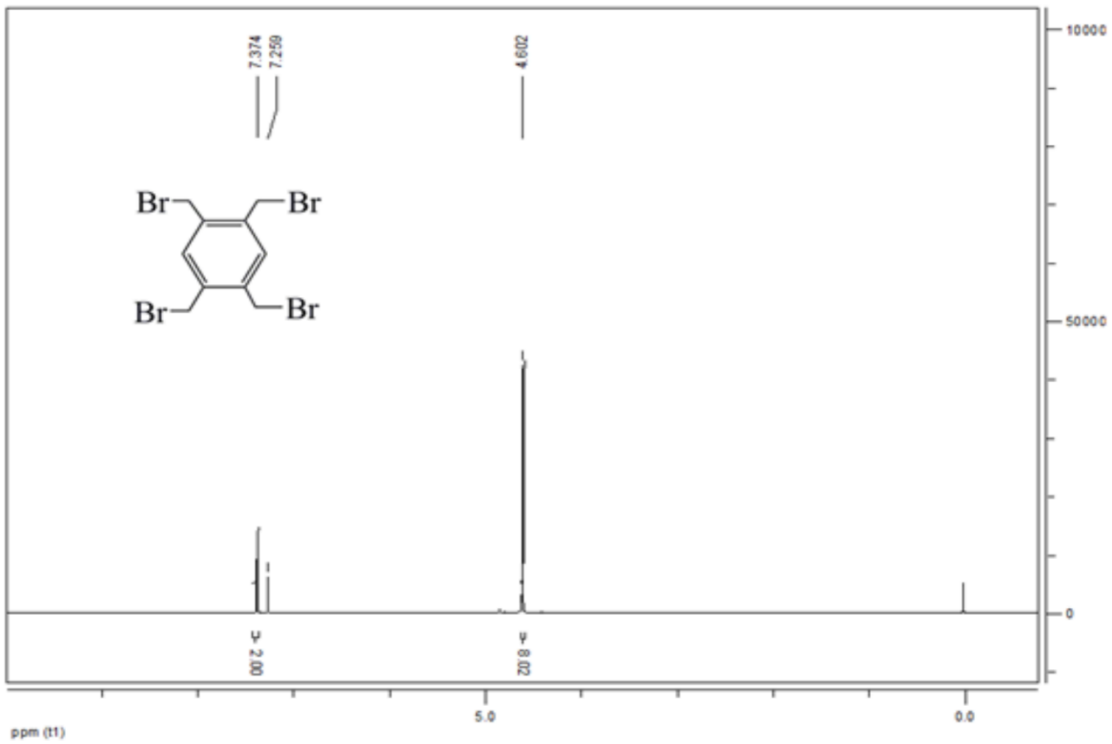

Fig. S25 The ^{1}H NMR (400 MHz, DMSO-d_6) spectrum of 1,2,4,5-tetra(bromomethyl)benzene.

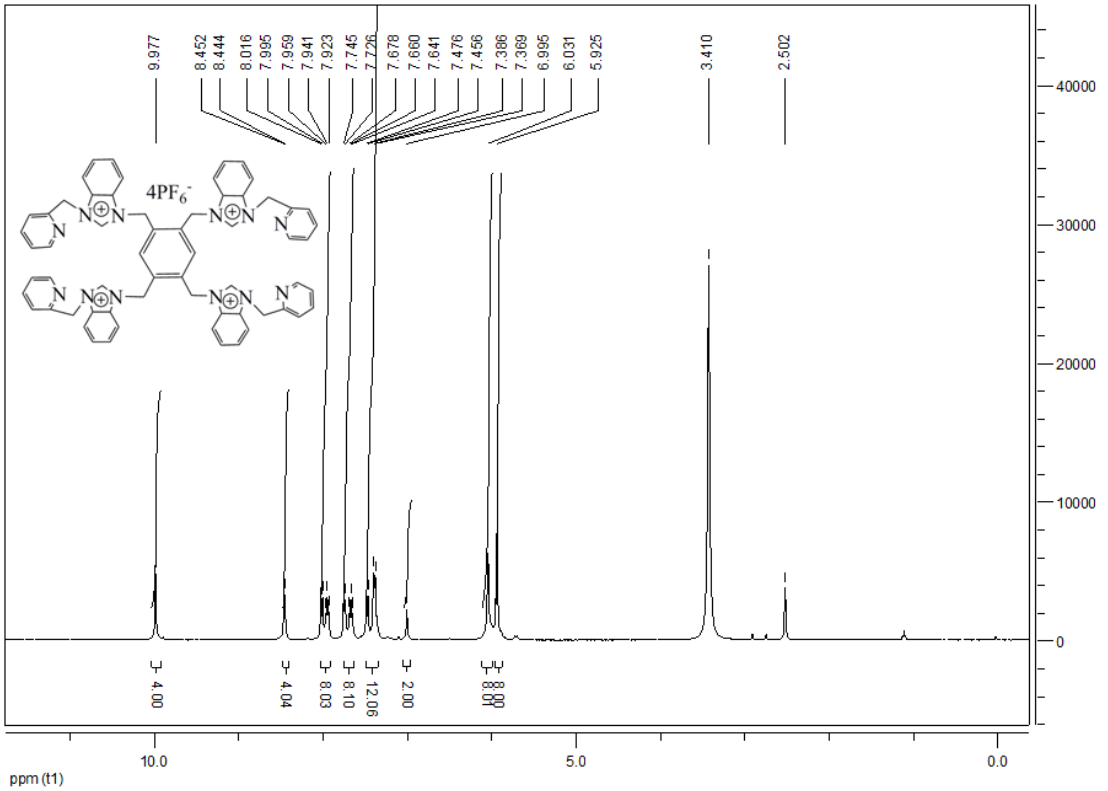

Fig. S26 The ^{1}H NMR (400 MHz, DMSO-d_6) spectrum of compound **1**.

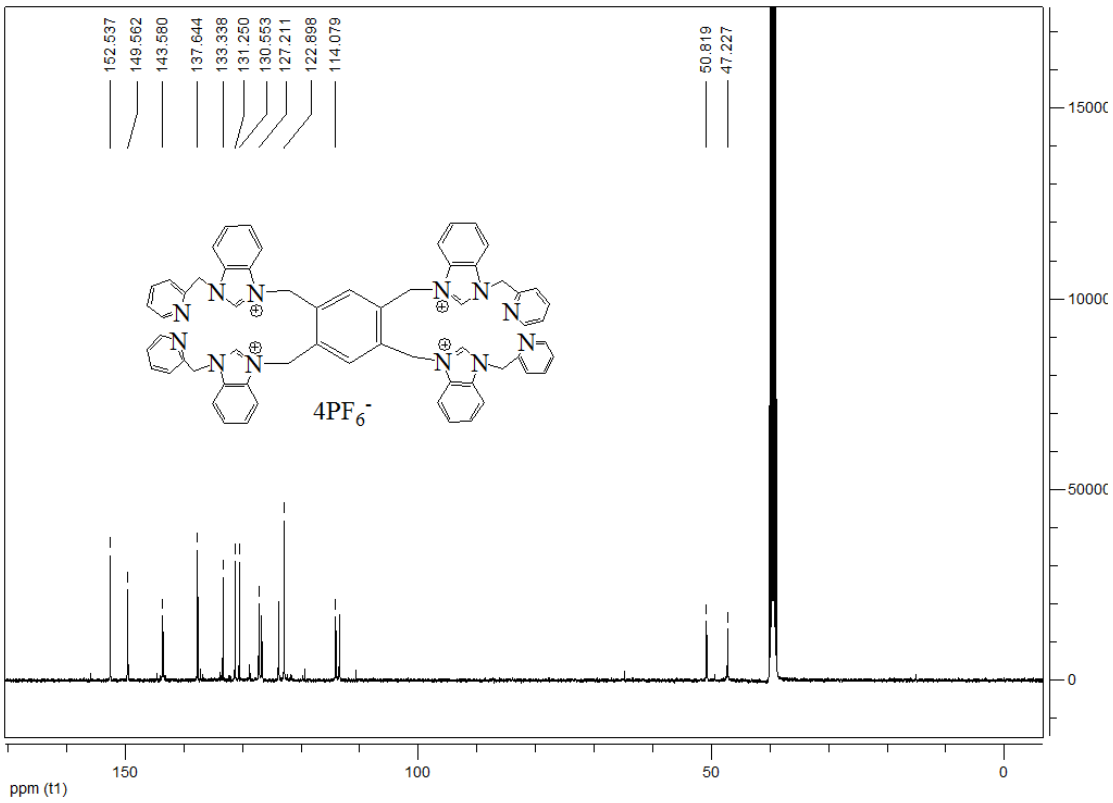

Fig. S27 The ^{13}C NMR (100 MHz, DMSO-d_6) spectrum of compound **1**.

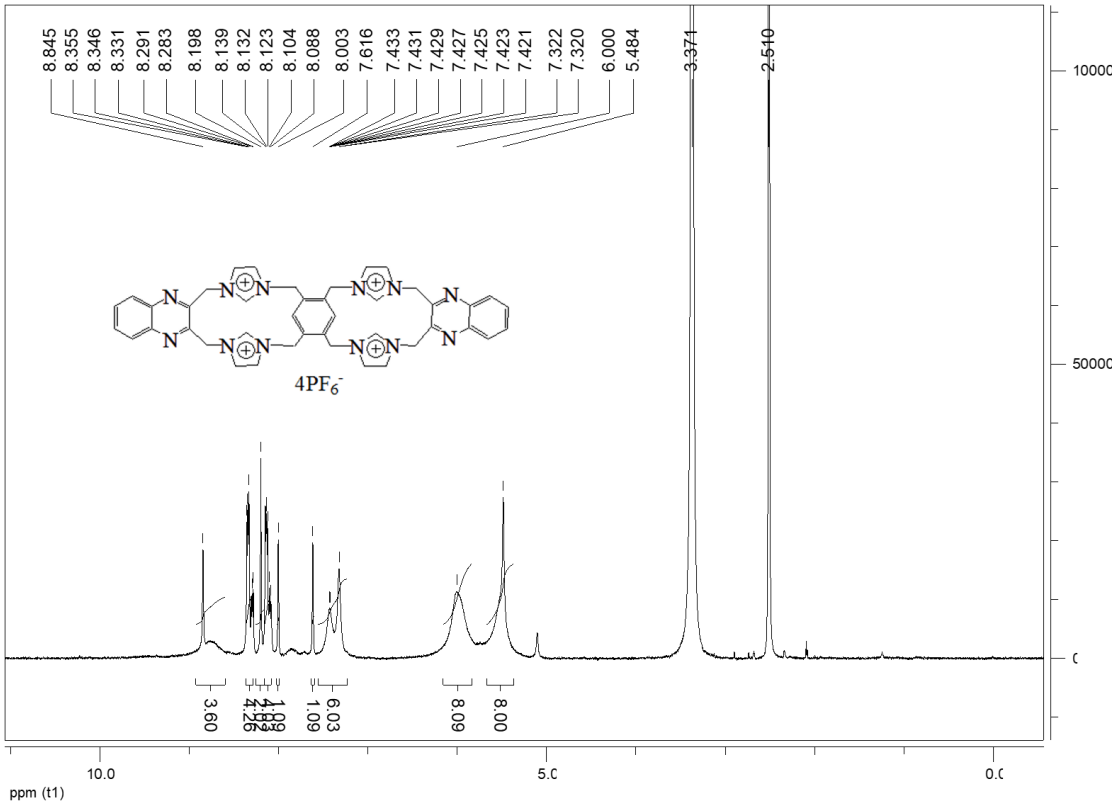

Fig. S28 The ^{1}H NMR (400 MHz, DMSO-d_6) spectrum of compound **2**.

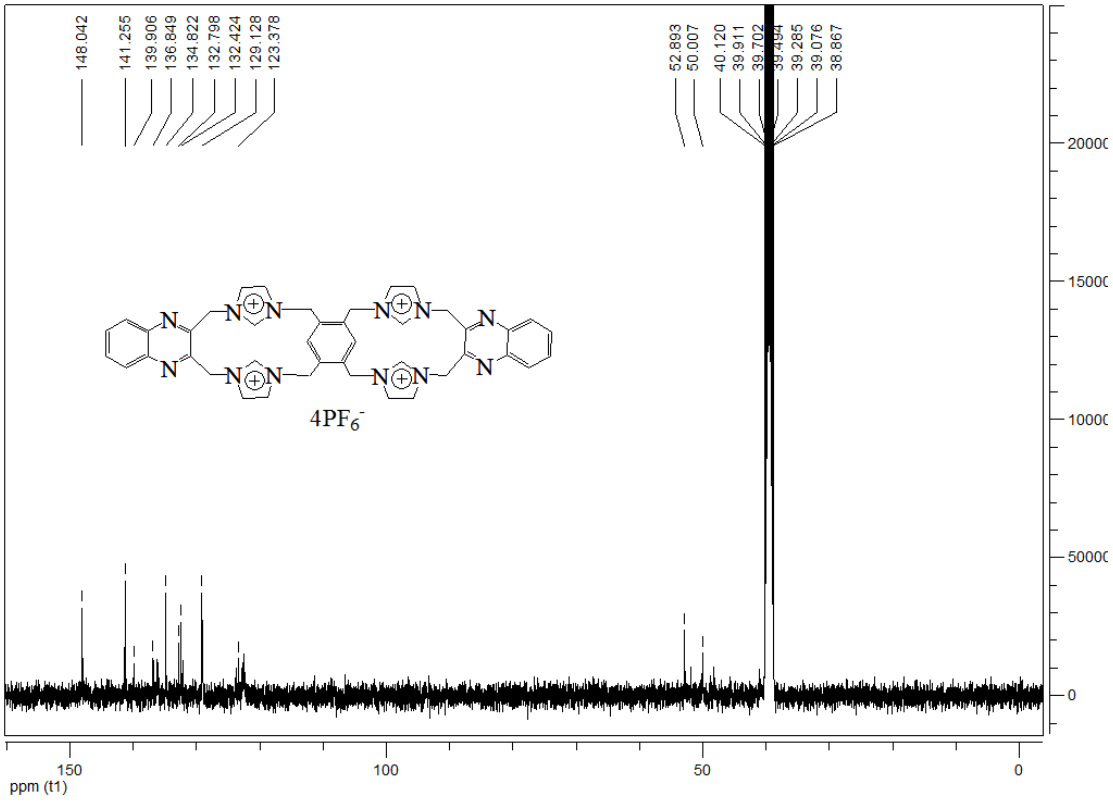

Fig. S29 The ^{13}C NMR (100 MHz, DMSO-d_6) spectrum of compound **2**.